

What shapes mesoscale wind anomalies in coastal upwelling zones?

Julien Boé · Alex Hall · François Colas ·
James C. McWilliams · Xin Qu · Jaison Kurian ·
Sarah B. Kapnick

Received: 12 March 2010 / Accepted: 25 February 2011 / Published online: 9 April 2011
© Springer-Verlag 2011

Abstract Observational studies have shown that mesoscale variations in sea surface temperature may induce mesoscale variations in wind. In eastern subtropical upwelling regions such as the California coast, this mechanism could be of great importance for the mean state and variability of the climate system. In coastal regions orography also creates mesoscale variations in wind, and the orographic effect may extend more than 100 km offshore. The respective roles of SST/wind links and coastal orography in shaping mesoscale wind variations in near-shore regions is not clear. We address this question in the context of the California Upwelling System, using a high-resolution regional numerical modeling system coupling the WRF atmospheric model to the ROMS oceanic model, as well as additional uncoupled experiments to quantify and separate the effects of SST/wind links and coastal orography on mesoscale wind variations. After taking into account potential biases in the representation of the strength of SST/wind links by the model, our results suggest that the magnitude of mesoscale wind variations arising from the orographic effects is roughly twice that of wind variations associated with mesoscale SST anomalies. This indicates that even in this region where coastal orography is complex and leaves a strong imprint on

coastal winds, the role of SST/winds links in shaping coastal circulation and climate cannot be neglected.

Keywords Mesoscale wind variations · Air sea interactions · California upwelling · Orographically-induced wind speed variations

1 Introduction

With roughly half the world's population, climate variability in coastal areas is associated with high socio-economic stakes. Yet simulating and predicting climate variability and changes in coastal areas is complex, due to air–sea interactions and sharp physiographic contrasts. For example, major coastal upwelling zones as the California Current System exhibit complex mesoscale dynamics. In this region, large scale wind during summer is generally equatorward and alongshore. The effect of coastal orography on large scale wind creates mesoscale variations in wind, and these variations may extend some distance offshore. In the California region such orographic effects are seen more than 100 km from shore (Winant et al. 1988; Enriquez and Friehe 1995; Edwards et al. 2002).

Though coastal orography may modulate and introduce mesoscale structure to the winds, their generally alongshore and equatorward direction generates coastal upwelling, resulting in a confined ribbon of colder ocean temperature nearshore. Eddies generated by dynamical instabilities of the currents (Marchesiello et al. 2003) lead to lateral heat transport, so that effects of coastal upwelling on sea surface temperature (SST) can be felt hundreds of km away (Capet et al. 2008).

Upwelling and the eddies associated with it potentially lead to complex air–sea interaction in coastal upwelling

J. Boé · A. Hall · X. Qu · S. B. Kapnick
Department of Atmospheric and Oceanic Sciences,
University of California, Los Angeles, CA, USA

J. Boé (✉)
URA 1875, CNRS/CERFACS, Toulouse, France
e-mail: boe@cerfacs.fr

F. Colas · J. C. McWilliams · J. Kurian
Institute of Geophysics and Planetary Physics,
University of California, Los Angeles, CA, USA

zones by introducing mesoscale structures in SSTs. Observational studies have shown that such mesoscale variations in SST are associated with mesoscale variations in wind. This link between SST and wind is found throughout the world ocean wherever there are strong SST fronts (see review by Xie 2004; Chelton et al. 2004; Small et al. 2008). Wind tends to accelerate (decelerate) over warmer (colder) SST, leading to approximately linear relations between wind stress curl (divergence) and cross-wind (downwind) SST gradients (Chelton et al. 2004; O'Neill et al. 2005). Both observational (Chelton et al. 2007, CSS07 in the following) and modeling (Haack et al. 2008; Seo et al. 2007) studies have shown evidence of SST influence on winds in the California upwelling zone.

The exact mechanisms responsible for SST influence on winds are still a subject of ongoing research. It has been hypothesized that it is linked to a modulation of vertical mixing within the marine atmospheric boundary layer by SST: Warm SST would cause enhanced vertical turbulent mixing, increasing downward mixing of horizontal momentum and therefore surface wind speed (Sweet et al. 1981; Jury and Walker 1988; Wallace et al. 1989; Song et al. 2009). However, Samelson et al. (2006) argue that this downward mixing mechanism cannot adequately explain the deceleration of wind over cold SST. Moreover, the pressure gradient, set up in response to the SST gradient through the front, may also play a role (Small et al. 2005; Spall 2007).

In coastal regions the situation is particularly complex, as both orography and SST shape mesoscale wind structures (Perlin et al. 2007), with a possible modulation of air-sea coupling by coastal orography. Indeed, Perlin et al. (in press) found weaker SST/wind links on the lee side of coastal capes compared to the upwind side. It is fundamental to better understand the nearshore wind structure as it plays a crucial role in shaping the nearshore upwelling dynamics (Capet et al. 2004) and the related oceanic mesoscale activity. Consequently it may have region-wide impacts through upscaling effects (Capet et al. 2008). Surface wind stress and upwelling must be in mutually-adjusted equilibrium on time scales longer than the oceanic dynamical adjustment time scale. The well-documented mesoscale effects of SST on wind therefore have the potential to play a large role in determining the mean state of the climate system in coastal upwelling zones. It is possible the typical magnitudes of mesoscale wind structures introduced by SST anomalies are comparable to those created by coastal orography. This would imply that the mean climate state in coastal upwelling zones can only be simulated and fully understood by invoking coupled ocean-atmosphere processes. The goal of this study is to determine whether this is the case by quantifying the respective roles of SST/wind links and coastal orography in shaping

mesoscale wind variations in coastal upwelling zones. Our testbed is the California current region, an upwelling zone adjacent to significant coastal orography.

The limitations of relevant observational data-sets make it difficult to address this question. Indeed, in situ observations of SST and wind are very sparse and satellite measurements may have some issues of spatial and/or temporal coverage. For example, the Quick Scatterometer (QuikSCAT) (Chelton and Freilich 2005) wind measurements are contaminated near shore (within about 30 km of land). In any case, even with perfect observations it would be difficult to separate effects of coastal orography and SST on wind nearshore based solely on observations. Such a separation is possible with numerical experiments. Given the scale of the processes involved, a very high resolution model is needed, suggesting a regional modeling approach. In this paper, we use the newly developed University of California, Los Angeles (UCLA)/Joint Institute for Regional Earth System Science and Engineering (JIFRESSE) Mesoscale Coupled Model (UMCM) to simulate the atmospheric-oceanic coupled system in the California upwelling region. This model couples the Regional Oceanic Modeling System (ROMS) to the Weather Research and Forecasting (WRF) atmospheric model. To separate effects of SST and coastal orography on mesoscale spatial variations of wind speed, additional uncoupled atmospheric simulations are also done in parallel.

The coupled model and numerical experiments are described in Sect. 2 and the model simulation is validated against observations in Sect. 3. The respective roles of SST and orography on mesoscale wind variations are studied in Sect. 4 and the realism of the strength of SST/wind links in the coupled model is analyzed in Sect. 5. Finally, the main results of our study are discussed and conclusions are drawn in Sect. 6.

2 Numerical experiments

UMCM consists of the Advanced Research WRF mesoscale atmospheric model coupled to the ROMS regional oceanic model. The WRF model (Skamarock et al. 2007) is a community mesoscale model designed for a wide range of applications. It consists of a fully compressible non-hydrostatic dynamical core with a run-time hydrostatic option and a full suite of physics enabling its use in a broad spectrum of applications across scales ranging from tens of meters to thousands of kilometers. The NOAA Land Surface Model is included in WRF (Chen and Dudhia 2001) to represent land surface processes. The parameterizations used for WRF in this study include the Rapid Radiative Transfer Model (RRTM) longwave radiation scheme (Mlawer et al. 1997), the Dudhia (1989) shortwave

radiation scheme, the WRF Single-Moment 3-class scheme microphysics scheme, and the Yonsei University planetary boundary layer scheme (Hong et al. 2006), a non-local k-profile scheme with an explicit treatment of entrainment processes at the top of the boundary layer. More information on the WRF model can be found on the WRF website (<http://www.wrf-model.org/index.php>).

ROMS (Shchepetkin and McWilliams 2005, 2009) solves the hydrostatic, free-surface primitive equations in 3D curvilinear coordinates that follow the bottom orography and sea level exactly (i.e., a generalized σ -coordinate), and the coastline approximately. ROMS contains accurate algorithms for extremum-preserving advection, the pressure-gradient force, the seawater equation of state compressibility, and split-explicit time-stepping for the barotropic/baroclinic mode coupling. It has been successfully tested in various applications to regional circulations in areas characterized by strong upwelling and mesoscale eddies (Blanke et al. 2002; Marchesiello et al. 2003; Capet et al. 2004, 2008; Colas et al. 2008). The ROMS-AGRIF version is used in the coupled model.

Coupling between WRF and ROMS is achieved in the following way: on a prescribed interval of 2 h, WRF sends wind stress, surface heat and water fluxes to ROMS time-averaged over the previous two hours. One hour later, and also with a prescribed interval of 2 h, ROMS sends time-averaged SST to WRF. The domains used in this study are shown in Fig. 1. The WRF domain contains two nests. The resolution of the outermost (innermost) nest is 36 km (12 km). The number of vertical levels is 35 in both two

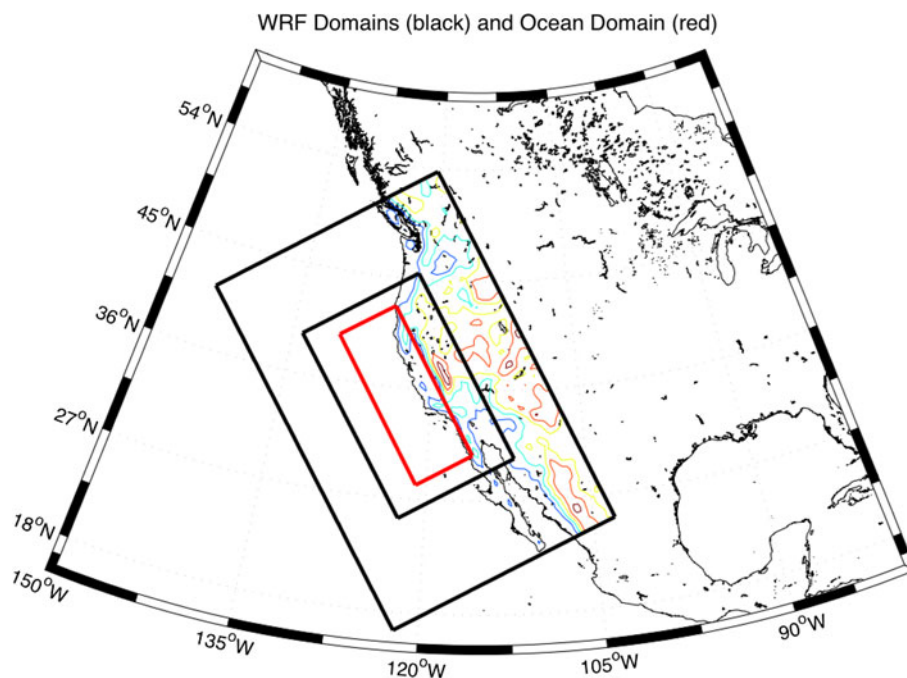
domains. The ROMS domain, with 32 vertical levels, is slightly smaller than WRF innermost nest and has a higher resolution of 4 km. The analyses of this paper are focused on the area encompassed by the ROMS domain, where WRF and ROMS are coupled. Results from ROMS are first interpolated to the WRF 12 km grid.

The lateral atmospheric boundary conditions for WRF are extracted from the 32 km resolution North America Regional Reanalysis (NARR, Mesinger et al. 2005) dataset. The lateral oceanic boundary conditions for ROMS come from the downscaling of the Simple Ocean Data Assimilation analysis (SODA, Carton et al. 2008) by an uncoupled nested ROMS simulation covering the Eastern North Pacific, with the ROMS to ROMS downscaling procedure described in Mason et al. (2009). The atmospheric forcing for this simulation is also extracted from the NARR reanalysis. Outside the ROMS domain, where WRF is not coupled to ROMS, SSTs from the uncoupled ROMS simulation are used as surface boundary conditions for WRF.

To isolate effects of coupling on the atmosphere solutions, an atmosphere-only WRF simulation forced by NARR as lateral and surface boundary conditions has been run. The domains are identical to the ones used for WRF in the coupled model. We denote this simulation as WRF-NARR. Note that although the resolution of NARR is 32 km, its SSTs are derived from a coarser 1 degree dataset.

The UCMC and WRF-NARR simulations have been run from November 2001 to October 2002. However, as

Fig. 1 Domains used in the coupled model: 36 and 12 km WRF domain in *black*, 4 km ROMS domain in *red*, where ROMS and WRF are coupled. The *contours* show the orography



SST/wind links are far stonger in the California region during summer (CSS07), the analyses presented here are for summer 2002 (defined as June to September).

3 Validation

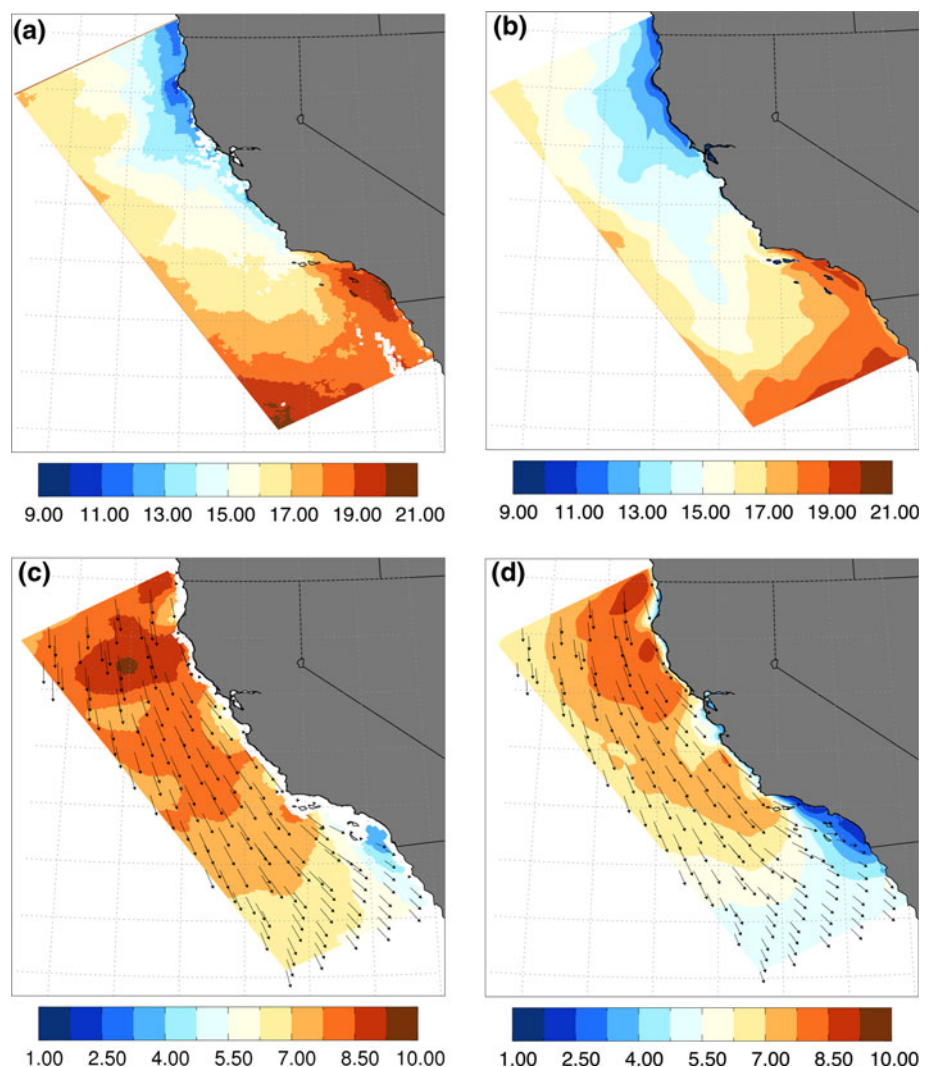
First, the results of the coupled simulation are compared to satellite and buoy observations. Buoy data are obtained from the National Buoy Data Center. Satellite wind observations come from QuikSCAT and SSTs from the Moderate-resolution Imaging Spectroradiometer (MODIS) (Walton et al. 1998).

Figure 2 shows the mean wind speed and SST during summer 2002, as simulated by the coupled model and measured by satellites. The coupled model captures the main spatial features of SST, in particular the cold SST near the Northern California shore associated with coastal upwelling. There is a moderate cold bias averaging 0.63 K

over the coupled domain. Observed winds are equatorward and alongshore, with a decrease in wind speed toward the south. This spatial pattern is captured by the coupled model. Simulated wind speeds in summer 2002 are smaller than the QuikSCAT ones by about 0.81 m s^{-1} (or 11%) averaged over the domain. As QuikSCAT winds are equivalent neutral winds and are compared to actual winds from the coupled model, this difference should not necessarily be interpreted as a bias of the model.

To validate in the nearshore zone, the coupled solution is compared to buoy data. The observed spatial pattern of mean wind speed nearshore during summer 2002 is reasonably well reproduced by the coupled model ($r = 0.75$, Fig. 3a). The mean bias of the coupled model compared to buoys is much smaller (0.09 m s^{-1}) than the difference with QuikSCAT computed previously over the entire domain. The spatial pattern of nearshore SST, with a general southward increase, is very well reproduced by the coupled model (Fig. 3b). However the comparison to buoy

Fig. 2 Mean SST ($^{\circ}\text{C}$) **a** measured by MODIS and **b** simulated by the coupled model, during summer 2002. Mean wind speed (m s^{-1}) **c** measured by QuikSCAT and **d** simulated by the coupled model, during summer 2002 (some *arrows* are suppressed for clarity of plotting). When more than 50% of the monthly daytime and nighttime values are missing in MODIS data, a missing value is used for the average (*white point*)



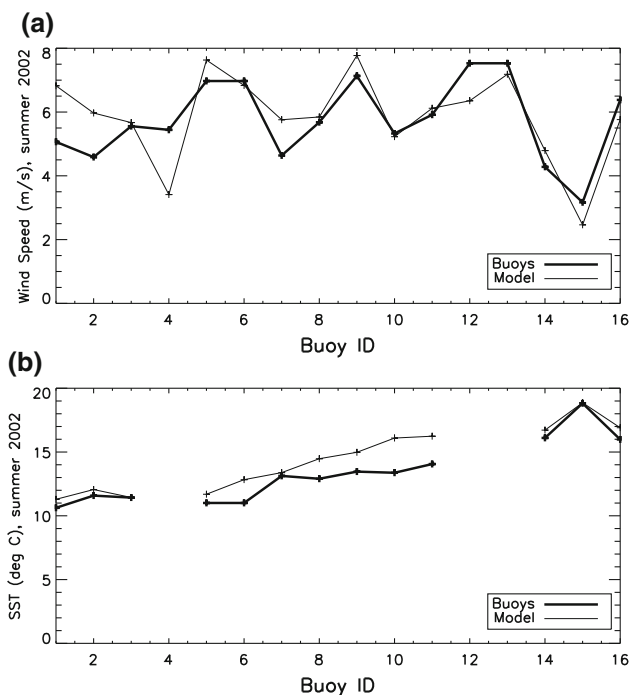


Fig. 3 Observed and simulated **a** mean wind speed (m s^{-1}) and **b** mean SST ($^{\circ}\text{C}$) during summer 2002 at each buoy location. The buoys are sorted on the plot from left to right given their latitudes (northernmost buoy on the left hand-side)

data reveals a slight warm bias in the coupled solution nearshore (0.94 K on average), in contrast with the cold bias in the average over the whole domain noted previously.

Daily correlations between 0.65 and 0.90 are obtained at most buoys for wind speed and daily correlations greater than 0.40 are obtained at most buoys for SST (Fig. 4). The spatial scale of synoptic flow patterns in the atmosphere is larger than the regional model domain, so that information describing the structure of individual atmospheric eddies is

contained within the lateral boundary conditions of the atmospheric component. In contrast, eddy variability in the California Current System has a smaller spatial scale than the ROMS domain. Since it is to a large extent intrinsic to the ocean (Marchesiello et al. 2003), one would not expect the oceanic component of the coupled model to reproduce the day-to-day variability associated with it. This likely explains the higher daily correlation between simulated and observed wind speed than between simulated and observed SSTs in the nearshore zone.

Despite some biases, the results in this section show that to the extent agreement is expected, the coupled model essentially reproduces basic characteristics of SST and wind on the domain of interest during summer 2002, even nearshore.

4 Roles of SST and orography

In this section, the respective roles of SST and orography in generating mesoscale wind variations are studied. First, SST and wind speed from UCMC and WRF-NARR are spatially high-pass filtered. The high-pass filter is designed to remove most of the spatial variations in NARR SST while retaining the mesoscale features of UCMC SST. The resulting fields for August 2002 are shown in Fig. 5. Note that some residual small-scale variations are seen in NARR SST after filtering. This arises from the SST interpolation procedure used in NARR. However, the amplitude of these variations is much smaller than the corresponding variations in UCMC SST and is neglected for the purposes of the analysis presented here.

Despite the near absence of mesoscale variations in NARR SST, wind speed in WRF-NARR exhibits strong mesoscale spatial variations along the California coast, in a band that extends more than 150 km offshore. This

Fig. 4 Daily correlations between observed and simulated **a** SST ($^{\circ}\text{C}$) and **b** wind speed (m s^{-1}) at different buoy locations. The model grid point corresponding to each buoy is chosen as that grid point centered less than a unit of atmospheric grid spacing (12 km) from each buoy with the highest daily correlation for wind speed

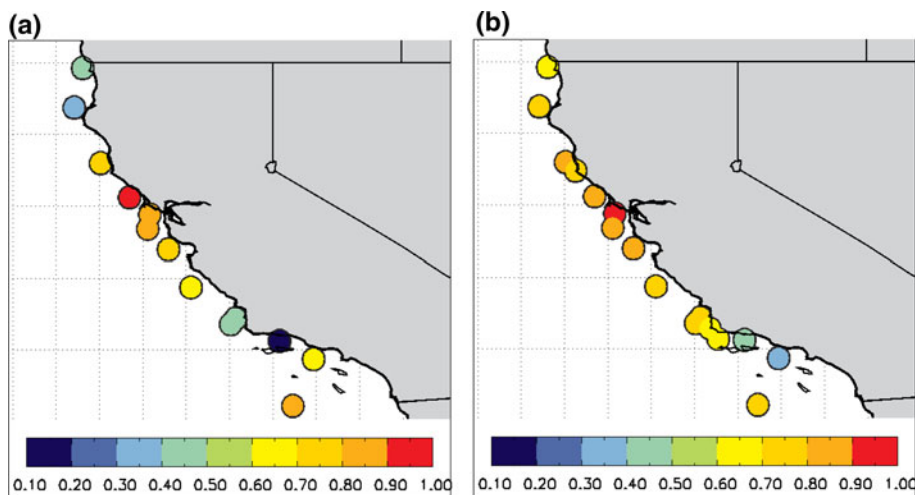
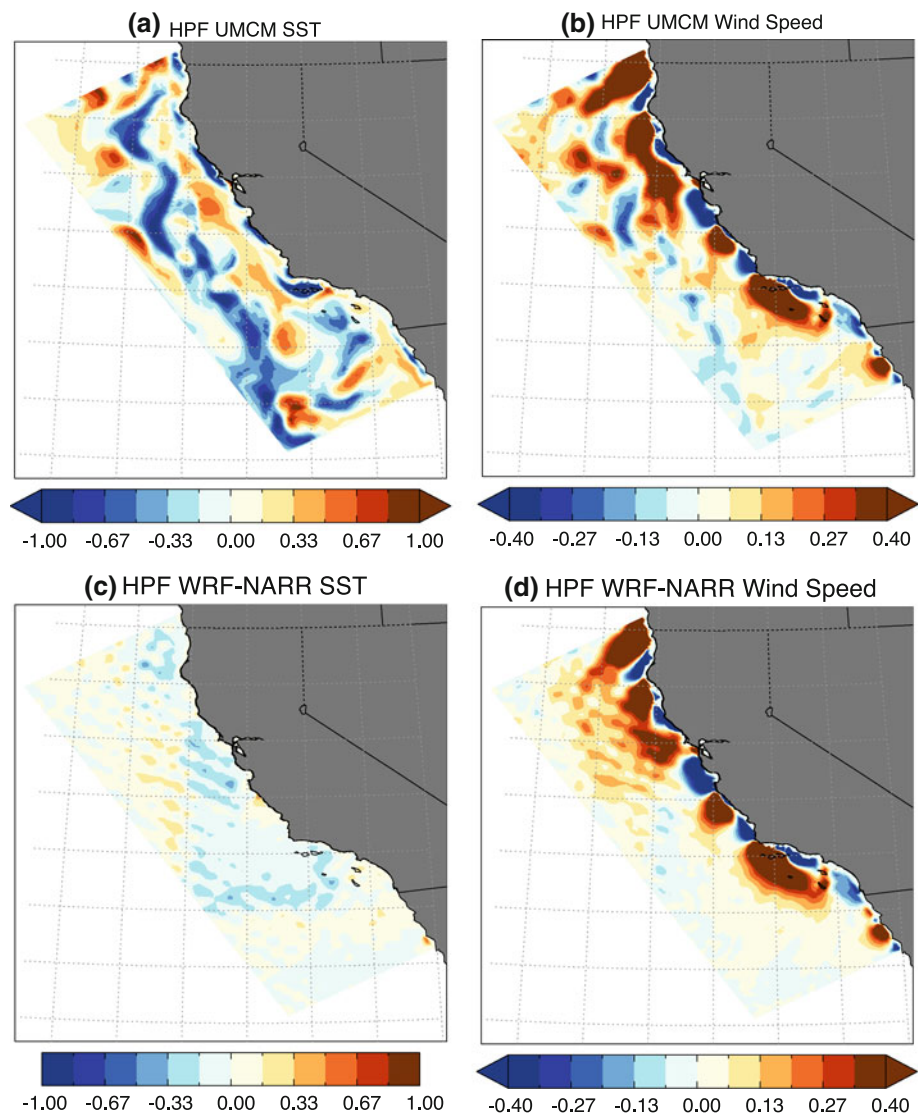


Fig. 5 Spatially high-pass filtered sea surface temperature (K) from **a** UCMC, **c** WRF-NARR and spatially high-pass filtered wind speed (m s^{-1}) from **b** UCMC, **d** WRF-NARR in August 2002. SST and wind speed from UCMC and WRF-NARR are spatially high-pass filtered by subtracting from those fields the large-scale fields calculated with a low-pass Loess filter with a cut-off window of 252 km by 252 km



nearshore mesoscale variability in wind speed is likely caused by the effect of coastal orography, as resolved by WRF, on large scale wind. Local maxima are seen downwind of Cape Mendocino, Point Sur and Point Conception while local minima are seen upwind of these coastal promontories. Note that in Fig. 2, these features are discernible in unfiltered wind fields, both in the coupled model and in QuikSCAT data. This reinforces our confidence that the simulated mesoscale structures in wind speed seen in Fig. 5b and d are realistic. Moreover, observational (Edwards et al. 2002) and numerical (Koracin and Dorman 2001) studies have already described such features along the coast of California. During summer, wind in this area is characterized by a steady equatorward alongshore direction. In these conditions, “compression bulges” of slower and deeper flow tend to form upwind of coastal promontories, while “expansion fans” of faster and thinner flow tend to develop downwind of the promontories

(Edwards et al. 2002). Nearshore, the mesoscale variations in UCMC wind speed are very similar to those simulated by WRF-NARR (Fig. 5). Conversely, offshore mesoscale features are seen in UCMC wind speed but not in WRF-NARR. In the coupled model these are probably related to mesoscale SST variations through the SST/wind links described in Sect. 1.

SST/wind links are further studied examining the three SST/wind relationships set forth by Chelton et al. (2004) and Song et al. (2009): (1) mesoscale wind speed anomalies should be proportional to mesoscale SSTs anomalies, (2) wind stress curl should be proportional to crosswind SST gradient, and (3) wind stress divergence should be proportional to downwind SST gradient. Wind stress rather than wind speed is used for (2) and (3) to facilitate the comparison of our results with previous studies (CSS07 in particular). The wind stress directly computed by WRF is used for this analysis. To evaluate relation (1), spatially

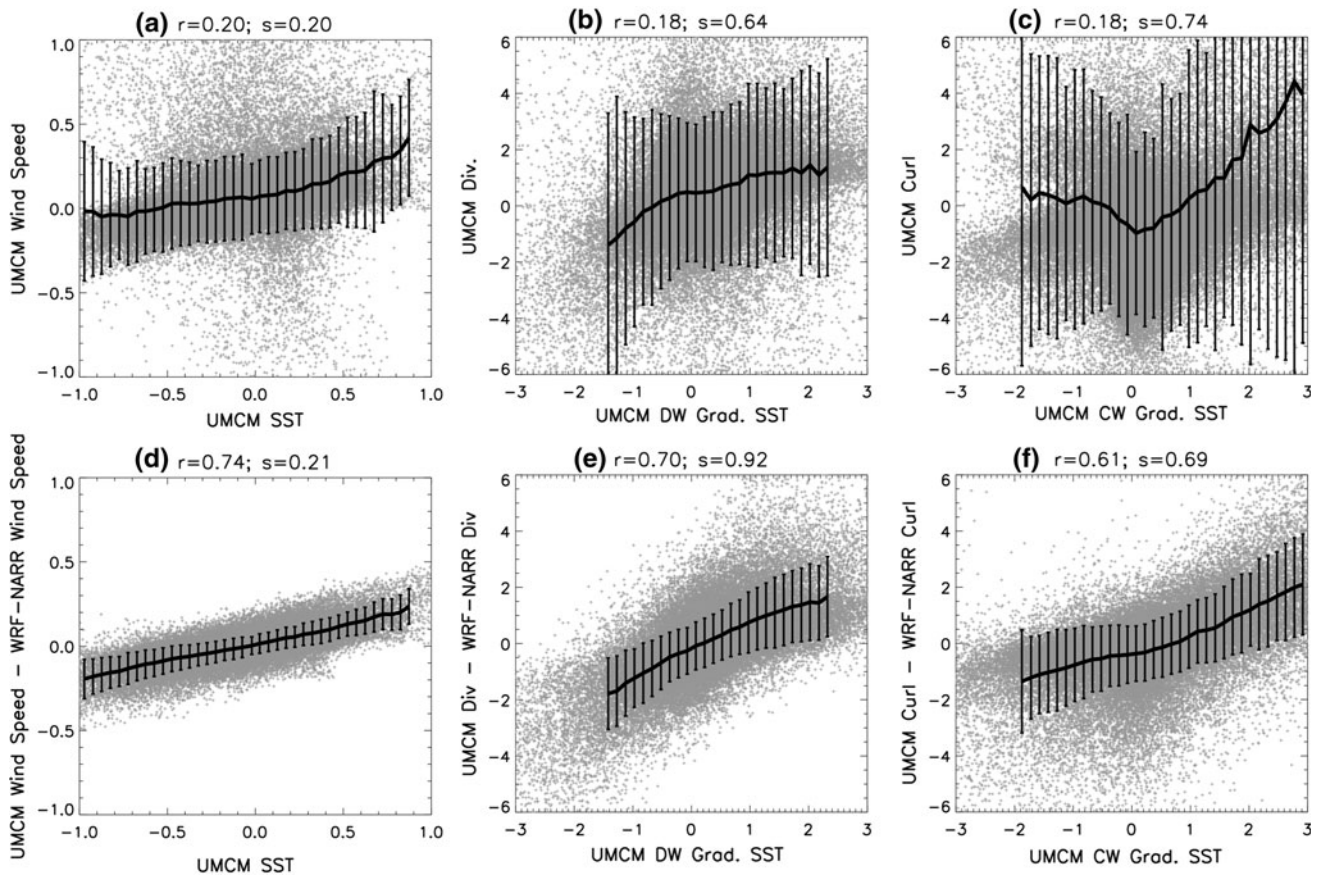


Fig. 6 **a** UCMC high-pass filtered wind speed (m s^{-1}) versus UCMC high pass filtered SST (K). **b** UCMC wind stress divergence ($\text{N m}^{-2} (10^4 \text{ km})^{-1}$) versus UCMC downwind SST gradient ($\text{K} (100 \text{ km})^{-1}$). **c** UCMC wind stress curl ($\text{N m}^{-2} (10^4 \text{ km})^{-1}$) versus UCMC crosswind SST gradient ($\text{K} (100 \text{ km})^{-1}$). **d** UCMC minus WRF-NARR high-pass filtered wind speed (m s^{-1}) versus UCMC high pass filtered SST (K). **e** UCMC minus WRF-NARR wind stress divergence ($\text{N m}^{-2} (10^4 \text{ km})^{-1}$) versus UCMC

downwind SST gradient ($\text{K} (100 \text{ km})^{-1}$). **f** UCMC minus WRF-NARR wind stress curl ($\text{N m}^{-2} (10^4 \text{ km})^{-1}$) versus UCMC crosswind SST gradient ($\text{K} (100 \text{ km})^{-1}$). The scatterplots show the fourteen 29-day averages at 7-day intervals for each ocean point. The *black line* is the binned average and the *error bars* stand for one standard deviation within each bin. The linear correlation (“r”) and slope (“s”) for the relationships are given at the top of each panel

high-pass filtered fields as shown in Fig. 5 are used. To evaluate relations (2) and (3), SST gradients, wind stress divergence and wind stress curl are calculated for each day on the original (i.e. unfiltered) fields. It is not necessary to spatially filter SST gradients or wind stress divergence and curl as those fields overwhelmingly exhibit mesoscale variations. As in CSS07, 29-day overlapping averages at 7 days interval are calculated (i.e. 14 temporal values during summer 2002) for the various relevant quantities in order to filter synoptic weather noise and clarify SST influence on surface winds.

The scatter plots obtained with the coupled model variables are shown in Fig. 6a–c. The three relationships that should result from SST/wind links are very weak, with correlations lower than 0.2. This raises the question of whether orographically-induced wind speed variations nearshore mask the effect of SST on wind speed. If this hypothesis is correct, SST/wind links should become much

more evident after removing orographic wind effects in UCMC.

To remove orographic effects in the coupled model output, we assume mesoscale wind variations in the coupled model result from the linear superposition of orographically-induced variations and those arising from wind/SST links. The results of the following analysis will indicate the extent to which this simple working hypothesis is justified. Effects of coastal orography on large scale wind should be identical in UCMC and WRF-NARR, as the same atmospheric domains and lateral boundary conditions are used for the two simulations. Orographically-induced wind variations are therefore estimated using the WRF-NARR simulation and removed from the total wind variations in the coupled model to obtain variations associated with SST/wind links. In other words, high-pass filtered wind speed, wind stress curl and divergence are computed from WRF-NARR as previously for UCMC and subtracted from

the same quantities computed from UCMC. Relations between these new quantities and spatially high-pass filtered SST, crosswind and downwind SST gradients from the coupled model are shown in scatterplots (Fig. 6d–f).

Once the effects of orography on wind are removed the scatter is reduced dramatically and the characteristic SST/wind links emerge, with correlation coefficients of 0.74, 0.70, 0.61 in Fig. 6d, e, f respectively. Given these results, the linear separation of the effects of SST and orography on wind seems to be an acceptable approximation to first order. Note that the slopes of the linear best fit to the relationships in Fig. 6e and f are smaller than the observational estimates given by CSS07 (1.92 and 2.59 vs. 0.69 and 0.92 respectively). This may be due either to an underestimate of the strength of SST/wind links in UCMC, or to the differences in periods and spatial domains between the two studies. This ambiguity is addressed in the next section. As found by previous studies, the slope of the relationship between downwind SST gradients and wind stress divergence is larger than the slope of the relationship between crosswind SST gradients and wind stress curl. O'Neill et al. (2010) showed that this difference is attributable to the fact that SST influences not only wind speed but also wind direction.

The previous analysis does not address possible spatial variations in the strength of SST/wind links. In particular, it would be interesting to know if the strength is identical nearshore (where the effect of orography on wind is strong) and offshore (where orographic effects are small). To study the spatial pattern of the strength of SST/wind links we consider the rectangular box of 20 points by 20 points surrounding each grid point, and compute the correlation and slope between spatially high pass filtered SST and wind speed within the box. If more than 60% of the points within a particular box are located over land, the values of the slope and correlation are considered missing. As previously, the fourteen 29-day averages at 7-day intervals

during summer 2002 are used (i.e. for each grid point, if the surrounding area is purely oceanic, the correlation and slope are computed based on $20 \times 20 \times 14$ values).

Figure 7a shows the correlation map obtained using high-pass filtered wind and SST from the coupled model. Nearshore, within about 150 km of land, the correlations are very small over most of the domain. This is consistent with our previous results demonstrating the masking effect of orography in mesoscale wind speed variations nearshore in the coupled model. As in the previous analysis, the orographically-induced wind speed variations, estimated using the WRF-NARR simulation, are now removed from UCMC high-pass filtered winds, and the correlation with UCMC high-pass filtered SST is re-computed (Fig. 7b). Once the effects of orography are removed, high correlations between wind speed and SST are obtained over all of the domain, even nearshore. The fact that this correlation is independent of the magnitude of orographic effects is further evidence that orographic effects and SST/wind links are linearly superposable as previously hypothesized. The map of the corresponding slope of the best fit to the SST/wind relationship is shown in Fig. 7c. Significant north-south variations are seen in the SST impact on winds, with values 2 or 3 times smaller in the south of the domain than in the north. Further research is needed to understand the physical origin of these spatial variations.

This analysis shows that SST/wind links exist in the model over the entire domain, even if it is partially masked by the orographic effects within roughly 150 km of the coastline.

5 Realism of the strength of SST/wind links

The previous analyses show that in the coupled model the effect of orography on mesoscale wind variations masks the effects of SST/wind links in the nearshore region. The

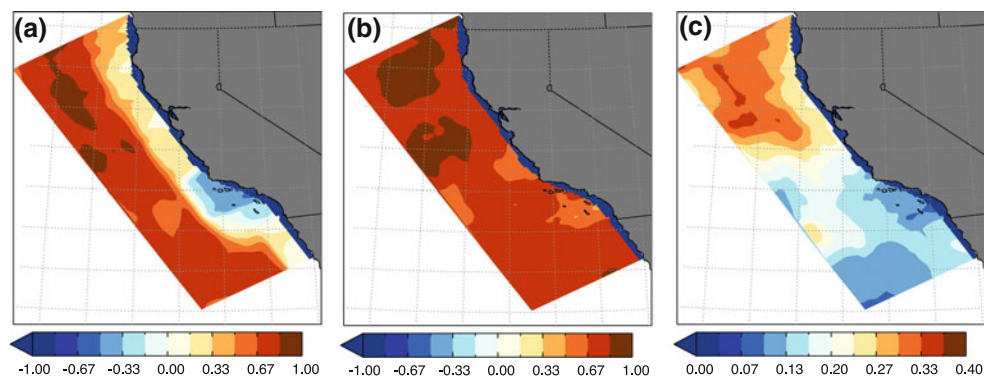


Fig. 7 **a** Running spatial correlation between spatially high-pass filtered wind speed and spatially high-pass filtered SST in the coupled model. **b** As **a** except that spatially high-pass filtered wind speed from

WRF-NARR has been removed from spatially high-pass filtered wind speed in the coupled model. **c** Slope corresponding to **b** ($\text{m s}^{-1} \text{K}^{-1}$). See text for details on the calculation

extent to which this conclusion is also reflective of the real world depends on the realism of the SST/wind links in the coupled model. Indeed, most models tend to underestimate the strength of SST/wind links (e.g. Chelton 2005; Maloney and Chelton 2006; Haack et al. 2008; Song et al. 2009; Bryan et al. 2010), often to a large extent (Seo et al. 2007). To evaluate the realism of the strength of SST/wind links in the coupled model, an observational estimate based on MODIS and QuikSCAT data is computed. Satellite data are first interpolated to the WRF innermost grid. The same spatial high-pass filter introduced in Sect. 4 is applied and the 4 monthly fields of summer 2002 are used for the calculation. (Calculations are done here on monthly quantities because the spatial coverage of MODIS SST over our domain of interest at the daily time step is very limited.)

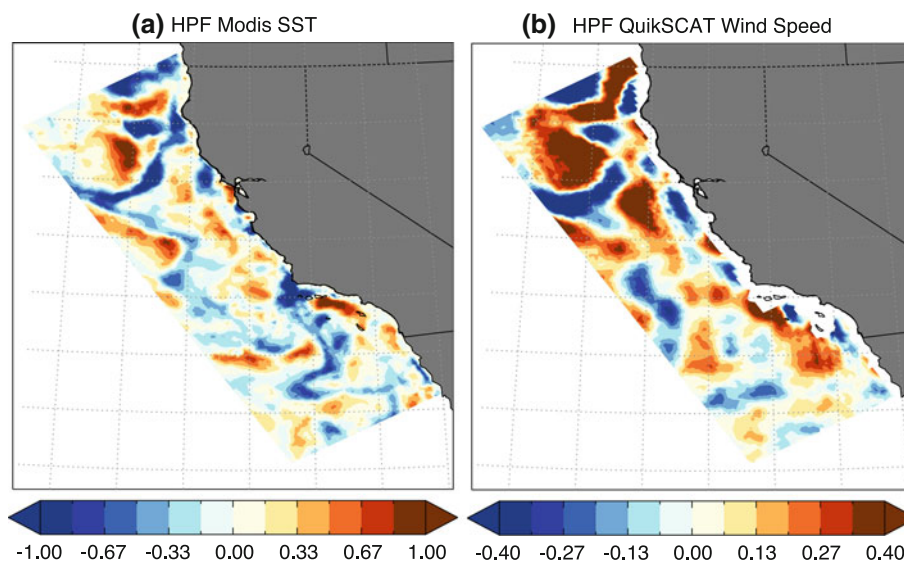
Figure 8 shows observed spatially high-pass filtered wind speed and SST in August 2002, and is to be compared to Fig. 5a and b. The most notable difference between model and observations is that observed mesoscale wind variations have comparable magnitudes nearshore and offshore (Fig. 8b), while simulated mesoscale wind anomalies are clearly larger nearshore (Fig. 5b). Moreover offshore mesoscale wind variations are generally larger in the observations. As offshore mesoscale wind variations are expected to be mostly due to SST/wind links, the comparison of Figs. 5b and 8b suggests that the strength of SST/wind links is underestimated in the coupled model. Orographic effects are seen in QuikSCAT winds nearshore, with local maxima (minima) upwind (downwind) of coastal promontories and unrelated to SST anomalies. These features are generally consistent with those seen in model simulations (Fig. 5b, d), despite some differences, for example south of Cape Mendocino. They may be partly due to the missing values in QuikSCAT near the coast. Indeed, the filtering of the points next to the missing values

cannot be strictly identical to the filtering in the coupled model. Moreover, SST mesoscale variations, largely intrinsic, are not identical in the coupled model and observations (Figs. 5a, 8a), and this may create differences in nearshore wind through SST/wind links. For example, the strong observed negative SST anomaly south of Cape Mendocino tends to reduce the positive wind anomaly associated with orographic effects.

The strength of the SST impact on winds is now computed only for the points further than 150 km from the coast to avoid the effect of orography on wind. Also, to avoid problems associated with missing values in MODIS during some months, only the points at a latitude greater than 32°N are used. The same methodology and region are also used to compute the strength of SST/wind links in the coupled model. The slope of the relation between mesoscale wind anomalies and mesoscale SST anomalies obtained using QuikSCAT and MODIS data is $0.42 \text{ m s}^{-1} \text{ K}^{-1}$ while the value obtained for the coupled model is $0.24 \text{ m s}^{-1} \text{ K}^{-1}$. Based on this diagnostic, the strength of SST/wind links is therefore underestimated by somewhat less than a factor of 2 in the coupled model.

To complete the comparison of SST/wind links in the coupled model and observations, the influence of SST gradients on wind stress curl and divergence is now quantified. As the downwind and crosswind components of SST gradients are nonlinear quantities, it is not desirable to compute them on monthly means and daily variables are necessary. Given the very poor spatial coverage of MODIS SST at the daily time step, here we use AMSR-E SST (Chelton and Wentz 2005), as in CSS07. The resolution of AMSR-E is coarser (56 km) but its spatial coverage each day is far better. Then, as is in Fig. 6, 29-day overlapping averages at 7 days interval of SST gradients, wind stress curl and divergence are computed. Figure 9 shows the

Fig. 8 **a** Spatially high-pass filtered sea surface temperature (K) from MODIS and **b** spatially high-pass filtered wind speed (m s^{-1}) from QuikSCAT in August 2002. The same spatial filter as in Fig. 5 is used



relations between SST gradients and wind stress curl and divergence in the observations and in the coupled model for the points further than 150 km from the coast. Correlations between wind stress curl (divergence) and crosswind (downwind) SST gradients are very similar in the model and observations but the slopes are roughly two times smaller in the coupled model, which is consistent with the previous result. Note that larger SST gradients are seen in the coupled simulation, which could be at least partly explained by the higher spatial resolution of the coupled simulation compared to AMSR-E data. Note further that the differences between observed coupling strengths computed here and in CSS07 are mainly due to the difference of spatial domains. When we use the same domain as CSS07, our values become almost identical to those in that study (not shown).

It is possible to assess whether the conclusion about the larger relative magnitude of the orographic effect on nearshore wind variations remains true given the underestimate of SST/wind links by UMCM. We do this by comparing the typical magnitudes of orographically-induced and SST-induced wind speed variations in the coastal zone, when the latter is scaled first by the simulated, and then by the observed strength of SST/wind links. First, the 4 monthly values of the standard deviation in space of high pass-filtered WRF-NARR wind speed are computed and their mean is taken. This is done only for points less

than 150 km from the coast. This quantity measures the pure effect of orography on mesoscale wind speed variations. A value of 0.43 m s^{-1} is obtained. Then, for the same coastal zone, high pass-filtered UMCM SST is multiplied by the strength of SST/wind links and the mean of the 4 monthly values of the standard deviation in space of this quantity is computed. This measure of the pure effect of SST on mesoscale wind speed variations nearshore depends on the strength of SST/wind links chosen. A value of 0.10 m s^{-1} is obtained for the simulated strength of $0.24 \text{ m s}^{-1} \text{ K}^{-1}$, while a value of 0.18 m s^{-1} is obtained for the observed strength computed with satellite data ($0.42 \text{ m s}^{-1} \text{ K}^{-1}$). Note that here we use offshore values for the SST/wind links strength for a nearshore region. This is an approximation, as for example, one can imagine that the strength of SST/wind links depends of the structure of the atmospheric boundary layer which varies along a line perpendicular to the coast. However, Fig. 7 indicates that at least in the coupled model these variations are rather limited throughout the domain. The simple analysis described in this section indicates that with a realistic strength of SST/wind links, the magnitude of wind speed variations associated with SST mesoscale variability becomes about half that of wind speed variations generated by coastal orography.

Some caveats are associated with this conclusion. First, crosswind SST gradients exhibit a larger scale organization

Fig. 9 **a** UMCM wind stress divergence ($\text{N m}^{-2} (10^4 \text{ km})^{-1}$) versus UMCM downwind SST gradient ($\text{K} (100 \text{ km})^{-1}$). **b** Observed wind stress divergence ($\text{N m}^{-2} (10^4 \text{ km})^{-1}$) versus observed downwind SST gradient ($\text{K} (100 \text{ km})^{-1}$). **c** UMCM wind stress curl ($\text{N m}^{-2} (10^4 \text{ km})^{-1}$) versus UMCM crosswind SST gradient ($\text{K} (100 \text{ km})^{-1}$). **d** Observed wind stress curl ($\text{N m}^{-2} (10^4 \text{ km})^{-1}$) versus observed crosswind SST gradient ($\text{K} (100 \text{ km})^{-1}$). The scatterplots show the fourteen 29-day averages at 7-day intervals for each ocean point. The *black line* is the binned average and the *error bars* stand for one standard deviation within each bin. The linear correlation (r) and slope (s) of the relationships are given at the top of each panel

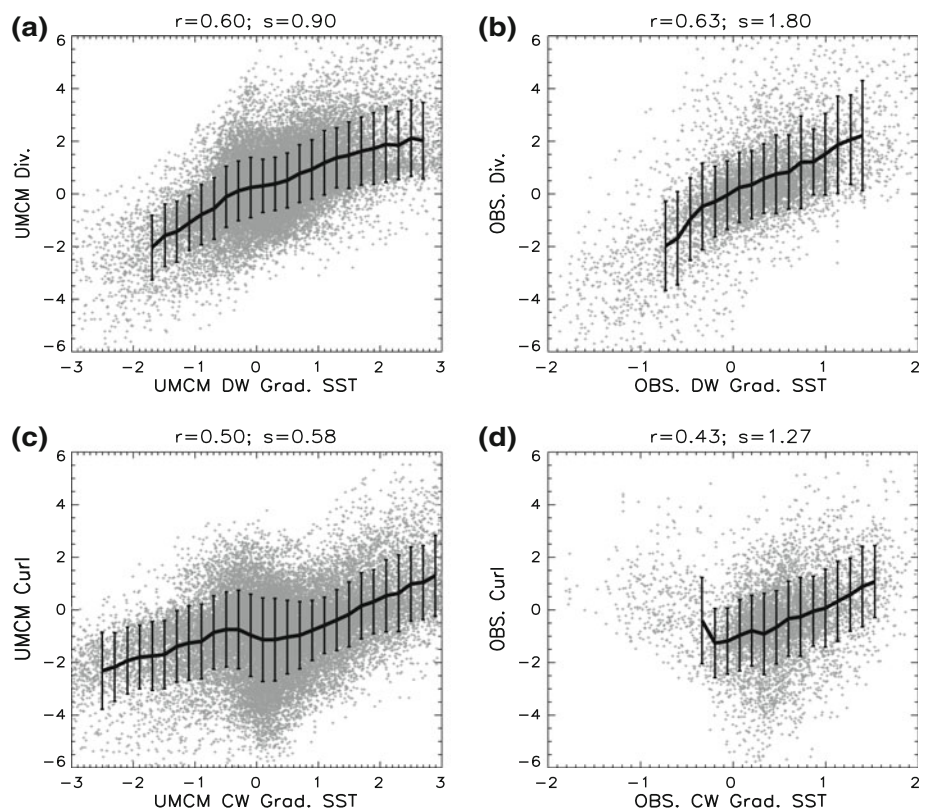
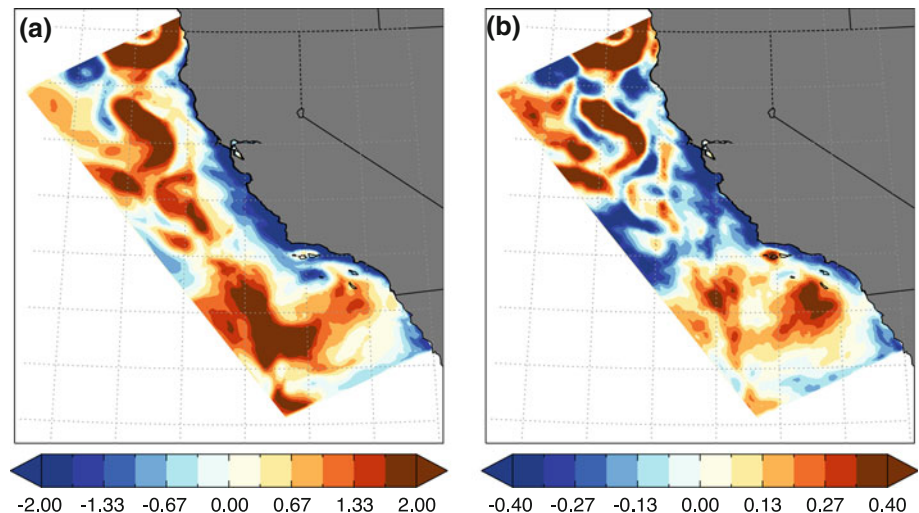


Fig. 10 Difference of **a** SST (K) and **b** wind speed (m s^{-1}) in August 2002 between WRF forced by SST from a climatological ROMS simulation at 4 km and the coupled model (forced simulation minus coupled simulation)



along California coast related to coastal upwelling. The resulting cross-shore gradient may have an important impact on mean wind stress curl nearshore through SST/wind links (Jin et al. 2009), while the previous analysis only deals with spatial variations nearshore. Second, it is possible the coupled model overestimates orographic effects on the spatial variability of nearshore wind. However, we do not have particular reasons to believe this to be the case, especially given the reasonable agreement of the coupled model's nearshore wind variations with observations (Sect. 3) We also made the implicit hypothesis that the coupled model's mesoscale SST variability is unbiased. An underestimate of the spatial variability of SST would lead to an underestimate of the role of SST/wind links. We saw in Sect. 3 that mean SST is too weak nearshore but too cool on average over the domain. This implies that the cold SST fronts related to coastal upwelling are somewhat underestimated in the coupled model and that therefore SST gradients and mesoscale variability nearshore may be too weak. Indeed, in August 2002, the spatial standard deviation of high-pass filtered SST for the points less than 150 km from the coast is 0.49 K in the observations and 0.38 K in the coupled model, an underestimate of roughly 25%. This suggests the ratio between orographic and SST/wind effects with a realistic value for strength of the SST/wind links is actually slightly smaller than 2. The respective roles of orography and SST/wind links in mesoscale wind variations are obviously sensitive to the spatial domain chosen, as the relative importance of SST/wind links compared to the orographic effect generally increases with distance from the coast. Finally, the relative importance of SST/wind links and orographic effects on mesoscale wind speed variations might vary spatially and from year to year, for example in response to variability in large-scale wind, strength of coastal upwelling or thickness of the marine atmospheric boundary layer.

With these caveats in mind, we conclude that although orographic effects likely dominate mesoscale wind structures in the nearshore zone, effects of SST/wind links are far from negligible, with an order of magnitude comparable to that of orographic effects, and therefore may play an important role in shaping coastal climate.

6 Discussion and conclusion

Using a high-resolution regional coupled model and a twin atmosphere-only experiment we studied the respective roles of orography and SST/wind links in the mesoscale spatial variability of wind in the California upwelling region. We found that in the coupled model, orographic effects are dominant within approximately 150 km of the coast. The strength of the links between SST and wind in the coupled model is underestimated by a factor 2, leading to an underestimate of the role of SST in mesoscale wind variations. However, simple calculations taking this underestimate into account suggest that the conclusion about the dominance of orography nearshore remains valid, though wind/SST links are certainly not negligible, with an order of magnitude comparable to that of orographic effects.

Some preliminary progress has been made in understanding why the strength of the SST impact on winds is underestimated in UCM. In the WRF uncoupled simulation forced by the 4 km ROMS SST described afterwards, the value of the regression coefficients between mesoscale winds and SST anomalies is very similar to that obtained with the coupled model. This result shows that the coupling procedure between the ocean and the atmosphere does not affect the simulated SST/wind links. The weakness of the wind/SST links is therefore due to simulated atmospheric processes. The boundary layer parameterization scheme as shown by Song et al. (2009) and the vertical

and horizontal resolution of WRF could be important in this respect. Future numerical experiments and analyses will investigate these points to improve the realism of the SST/winds links in UCMC.

Even if the effect of orography on mesoscale wind variations is somewhat larger nearshore, SST/wind effects may be competitive, and furthermore may play a significant role in coastal atmospheric and oceanic circulation. To illustrate this point, we use the results of an additional uncoupled WRF simulation over the 2001–2002 period forced by NARR lateral boundary conditions and by SST from an uncoupled climatological ROMS simulation. The SST boundary condition is the only difference between this uncoupled WRF simulation and the coupled run analyzed in the main part of this paper. This ROMS simulation supplying the lower boundary condition has a 4 km resolution and is forced by monthly climatologies of wind stress from QuikSCAT and of heat fluxes from the Comprehensive Ocean-Atmosphere Data Set (COADS). Figure 10 shows the difference of SST and wind speed between the coupled simulation and this uncoupled WRF simulation in August 2002. Nearshore, the uncoupled simulation exhibits colder SST (around 2.5 K) in a region centered around Point Conception, linked to stronger upwelling in the uncoupled ROMS experiment compared to the coupled model. Consistent with effects of SST/wind links, wind speed is also smaller in this area by roughly 0.6 m s^{-1} (or equivalently by about 10%). If the model had SST/wind links matching the observations, the wind speed in the uncoupled WRF run would likely be about 20% smaller. Note also that effects of SST/wind links explain most of the differences in the spatial variations of wind speed between the results of the two simulations over all of the domain: the spatial correlation between the differences of wind speed and the differences of SST is 0.79. The decrease in wind velocity nearshore linked to colder SST would in turn reduce coastal upwelling in a coupled system and SST-induced change in wind stress curl would strengthen offshore upwelling through Ekman pumping (Jin et al. 2009). This suggestion of a feedback among SST, upwelling and alongshore wind indicates the utility of using an ocean-atmosphere coupled model to study this region.

Acknowledgments This work was supported by the US National Science Foundation (NSF 0747533). Opinions, findings, conclusions, or recommendations expressed here are those of the authors and do not necessarily reflect NSF views. This research was supported in part by the National Science Foundation through TeraGrid resources provided by the Pittsburgh Supercomputing Center. We acknowledge the WRF and ROMS development groups and Hartmut Frenzel who helped with the implementation of the coupled model. NARR data from the US National Centers for Environmental Prediction were provided by the Data Support Section of the Computational and Information Systems Laboratory at the National Center for

Atmospheric Research. NCAR is supported by grants from the National Science Foundation. QuikSCAT data are produced by Remote Sensing Systems and sponsored by the NASA Ocean Vector Winds Science Team. AMSR-E data are produced by Remote Sensing Systems and sponsored by the NASA Earth Science MEASURES DISCOVER Project and the AMSR-E Science Team. Data are available at <http://www.remss.com>. The MODIS SST data were obtained from the Physical Oceanography Distributed Active Archive Center (PO.DAAC) at the NASA Jet Propulsion Laboratory, Pasadena, CA. <http://www.podaac.jpl.nasa.gov>.

References

- Blanke R, Roy C, Penven P, Speich S, McWilliams JC, Nelson G (2002) Linking wind and interannual upwelling variability in a regional model of the southern Benguela. *Geophys Res Lett* 29(24):2188. doi:10.1029/2002GL015718
- Bryan FO, Tomas R, Dennis JM, Chelton DB, Loeb NG, McClean JL (2010) Frontal scale air-sea interaction in high-resolution coupled climate models. *J Clim* 23(23):6277–6291
- Capet XJ, Marchesiello P, McWilliams JC (2004) Upwelling response to coastal wind profiles. *Geophys Res Lett* 32:L13311. doi:10.1029/2004GL020123
- Capet X, Colas F, Penven P, Marchesiello P, McWilliams J (2008) Eddies in eastern-boundary subtropical upwelling systems. In: Hecht M, Hasumi H (eds) *Eddy-resolving ocean modeling*. AGU Monograph, vol 177, Washington, p 350
- Carton JA, Giese BS (2008) A reanalysis of ocean climate using simple ocean data assimilation (SODA). *Mon Weather Rev* 136:2999–3017
- Chelton DB (2005) The impact of SST specification on ECMWF surface wind stress fields in the eastern tropical Pacific. *J Clim* 18:530–550
- Chelton DB, Freilich MH (2005) Scatterometer-based assessment of 10-m wind analyses from the operational ECMWF and NCEP numerical weather prediction models. *Mon Weather Rev* 133:409–429
- Chelton DB, Wentz FJ (2005) Global microwave satellite observations of sea surface temperature for numerical weather prediction and climate research. *Bull Am Meteorol Soc* 86:10971115
- Chelton DB, Schlax MG, Freilich MH, Milliff RF (2004) Satellite measurements reveal persistent small-scale features in ocean winds. *Science* 303:978–983
- Chelton DB, Michael GS, Roger MS (2007) Summertime coupling between sea surface temperature and wind stress in the California current system. *J Phys Oceanogr* 37(3):495–517
- Chen F, Dudhia J (2001) Coupling an advanced land-surface/hydrology model with the Penn State/NCAR MM5 modeling system. Part I: model description and implementation. *Mon Weather Rev* 129:569–585
- Colas F, Capet X, McWilliams JC, Shchepetkin A (2008) 1997/1998 El Niño off Peru: a numerical study. *Prog Oceanogr* 79:138–155
- Dudhia J (1989) Numerical study of convection observed during the winter monsoon experiment using a mesoscale two-dimensional model. *J Atmos Sci* 46:3077–3107
- Edwards KA, Rogers DP, Dorman CE (2002) Adjustment of the marine atmospheric boundary layer to the large-scale bend in the California coast. *J Geophys Res* 107:3213. doi:10.1029/2001JC000807
- Enriquez AG, Friehe CA (1995) Effects of wind stress and wind stress curl variability on coastal upwelling. *J Phys Oceanogr* 25:1651–1671
- Haack T, Chelton D, Pullen J, Doyle JD, Schlax M (2008) Air-sea interaction from US west coast summertime forecasts. *J Phys Oceanogr* 38:2414–2437

- Hong SY, Noh Y, Dudhia J (2006) A new vertical diffusion package with an explicit treatment of entrainment processes. *Mon Weather Rev* 134:2318–2341
- Jin X, Dong C, Kurian J, McWilliams JC, Chelton DB, Li Z (2009) SST/wind interaction in coastal upwelling: oceanic simulation with empirical coupling. *J Phys Oceanogr* 39(11):2957–2970
- Jury MR, Walker N (1988) Marine boundary layer modification across the edge of the Agulhas Current. *J Geophys Res* 93:647–654
- Koracin D, Dorman CE (2001) Marine atmospheric boundary layer divergence and clouds along California in June 1996. *Mon Weather Rev* 129:2040–2055
- Maloney ED, Chelton DB (2006) An assessment of the sea surface temperature influence on surface wind stress in numerical weather prediction and climate models. *J Clim* 19(12):2743–2762
- Marchesiello P, McWilliams JC, Shchepetkin A (2003) Equilibrium structure and dynamics of the California current system. *J Phys Oceanogr* 33:753–783
- Mason E, Molemaker J, Colas F, Shchepetkin A, McWilliams JC, Sangra P (2009) Procedures for offline grid nesting in regional ocean models. *Ocean Model* (submitted)
- Mesinger F, Dimego G, Kalnay E, Mitchell K, Shafran PC, Ebisuzaki W, Jovic D, Woollen J, Rogers E, Berbery EH, Ek MB, Yun F, Grumbine R, Higgins W, Hong Li, Ying L, Manikin G, Parrish D, Wei S (2006) A long-term, consistent, high-resolution climate dataset for the North American domain, as a major improvement upon the earlier global reanalysis datasets in both resolution and accuracy, is presented. *Bull Am Meteorol Soc* 87(3):342–360
- Mlawer E, Taubman S, Brown P, Lacono M, Clough S (1997) Radiative transfer for inhomogeneous atmosphere: RRTM, a validated correlated-k model for the longwave. *J Geophys Res* 102:16663–16682
- O’Neill LW, Chelton DB, Esbensen SK, Wentz FJ (2005) High-resolution satellite observations of SST modification of the marine atmospheric boundary layer over the Agulhas Return Current. *J Clim* 18:2706–2723
- O’Neill LW, Chelton DB, Esbensen SK (2010) The effects of SST-induced surface wind speed and direction gradients on midlatitude surface vorticity and divergence. *J Clim* 23(2):255–281
- Perlin N, Skillingstad ED, Samelson RM, Barbour PL (2007) Numerical simulation of air-sea coupling during coastal upwelling. *J Phys Oceanogr* 37:2081–2093
- Perlin N, Skillingstad ED, Samelson RM (in press) Coastal atmospheric circulation around an idealized cape during wind-driven upwelling studied from a coupled ocean-atmosphere model. *Mon Weather Rev*
- Samelson RM, Skillingstad ED, Chelton DB, Esbensen SK, O’Neill LW, Thum N (2006) On the coupling of wind stress and sea surface temperature. *J Clim* 19:1557–1566
- Seo H, Miller AJ, Road JO (2007) The Scripps coupled ocean atmosphere regional (SCOAR) model, with applications in the eastern Pacific sector. *J Clim* 20:381–402
- Shchepetkin AF, McWilliams JC (2005) The regional oceanic modeling system (ROMS): a split-explicit, free-surface, topography-following-coordinate oceanic model. *Ocean Model* 9:347–404
- Shchepetkin AF, McWilliams JC (2009) Correction and commentary for “Ocean forecasting in terrain-following coordinates: formulation and skill assessment of the Regional Ocean Modeling System” by Haidvogel et al. *J Comp Phys* 227:3595–3624
- Skamarock WC, Klemp JB, Dudhia J, Gill DO, Barker DM, Wang W, Powers JG (2007) A description of the advanced research WRF version 2. NCAR/TN-468+STR. NCAR technical note, 88 pp
- Small RJ, Xie S-P, Wang Y, Esbensen SK, Vickers D (2005) Numerical simulation of boundary layer structure and cross-equatorial flow in the eastern Pacific. *J Atmos Sci* 62:1812–1830
- Small RJ, deSzoeke SP, Xie SP, O’Neill L, Seo H, Song Q, Cornillon P, Spall M, Minobe S (2008) Air-sea interaction over ocean fronts and eddies. *Dyn Atmos Oceans* 45(3–4):274–319
- Song Q, Chelton DB, Esbensen SK, Thum N, O’Neil LW (2009) Coupling between sea-surface temperature and low-level winds in mesoscale numerical models. *J Clim* 22(1):146–164
- Spall M (2007) Midlatitude wind stress-sea surface temperature coupling in the vicinity of oceanic fronts. *J Clim* 20:3785–3801
- Sweet WR, Fett R, Kerling J, La Violette P (1981) Air-sea interaction effects in the lower troposphere across the north wall of the Gulf Stream. *Mon Weather Rev* 109:1042–1052
- Wallace JM, Mitchell TP, Deser C (1989) The influence of sea surface temperature on surface wind in the eastern equatorial Pacific: seasonal and interannual variability. *J Clim* 2(12):1500–1506
- Walton CC, Pichel WG, Sapper JF (1998) The development and operational application of nonlinear algorithms for the measurement of sea surface temperatures with the NOAA polar-orbiting environmental satellites. *J Geophys Res* 103(C12):27999–28012
- Winant CD, Beardsley R, Dorman C, Friehe C (1988) The marine layer off northern California: an example of supercritical channel flow. *J Atmos Sci* 45:3588–3605
- Xie SP (2004) Satellite observations of cool ocean-atmosphere interaction. *Bull Am Meteorol Soc* 85:195–208